UCRL- 100710
PREPRINT

Bragg Crystal Polarimeters

E. Silver
A. Simionivici
S. Labov
R. Novick
P. Kaaret
C. Martin
T. Hamilton
M. Weisskopf
R. Elsner
J. Beeman
G. Chanan
G. Manzo
E. Costa
G. Perola
G. Fraser

This paper was prepared for submittal to
SPIE's 33rd Annual International Symposium Proceedings
San Diego, CA, August 6-11, 1989

June 15, 1989

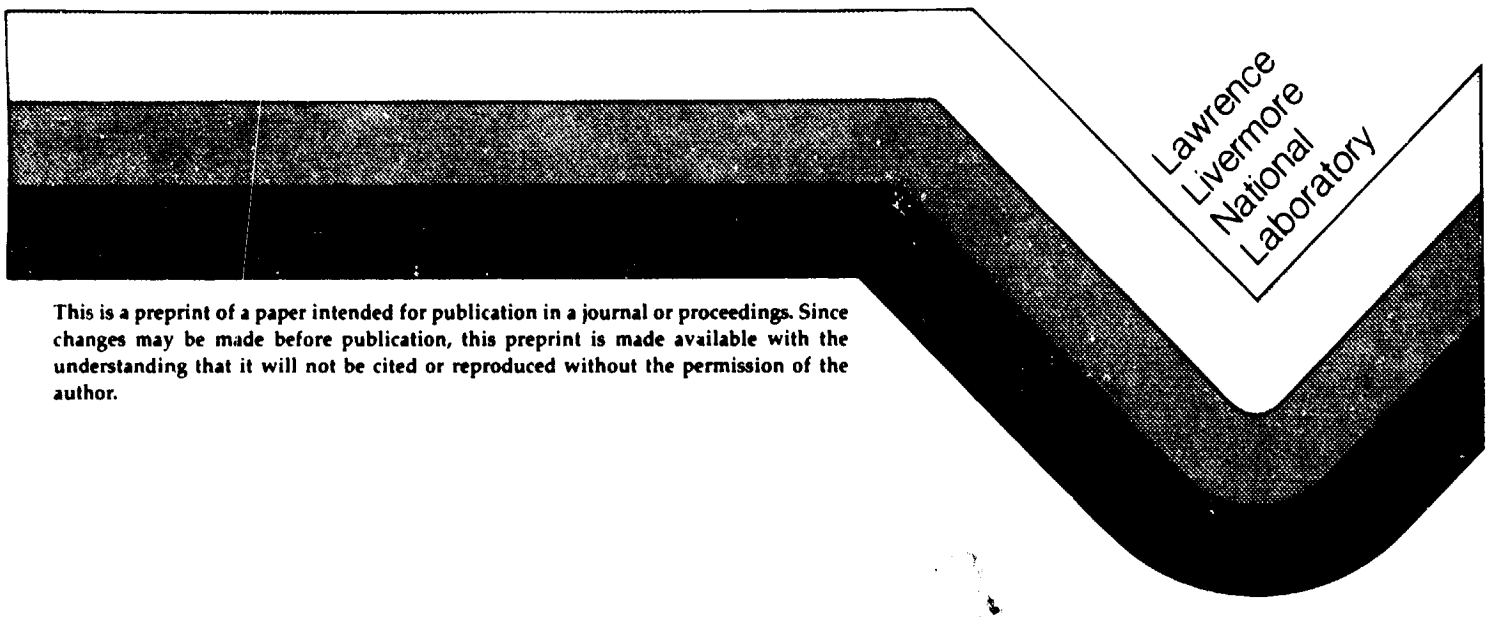

UCRL--100710

DE89 015775

Bragg crystal polarimeters*

E. Silver
A. Simionivici and S. Labov
Laboratory For Experimental Astrophysics
Lawrence Livermore National Laboratory, Livermore, California 94550

R. Novick, P. Kaaret, C. Martin and T. Hamilton
Columbia Astrophysics Laboratory

M. Weisskopf and R. Elsner
NASA Marshall Space Flight Center

J. Beeman
Lawrence Berkeley National Laboratory

G. Chanan
University of California, Irvine

G. Manzo , E. Costa, and G. Perola
IFCAI/CNR, Istituto di Astrofisica Spaziale, and University of Rome (Italy)

G. Fraser
University of Leicester (UK)

ABSTRACT

A Bragg crystal oriented at 45° to an incoming beam of x-rays acts as a polarization analyzer. This crystal geometry preferentially reflects those x-rays which satisfy the Bragg condition and whose electric vectors are perpendicular to the plane defined by the incident and reflected photons. X-rays with electric vectors parallel to this plane of incidence are photoelectrically absorbed. The energy bandwidth of nearly perfect crystals is extremely small which makes them very inefficient x-ray polarimeters. This limitation is particularly acute for observations of the relatively weak x-ray continuum of stellar sources. The bandwidth can be greatly increased by employing mosaic or ideally imperfect crystals. Mosaic crystals possess a high integrated reflectivity which results in a large increase in the reflection of continuum radiation. A review of the theory and performance characteristics of crystal polarimeters designed for observations of cosmic x-ray sources is presented.

1. INTRODUCTION

In this report we review the basic aspects of Bragg crystal diffraction theory that are relevant to the design of a crystal polarimeter with optimum sensitivity for observing stellar x-ray sources above the energy of 1 keV. We will show how these principles were incorporated in the OSO-8 polarimeter which provided the most successful measurements of cosmic x-ray polarization reported to date [1,2]. Our discussion subsequently highlights pertinent aspects of x-ray diffraction theory for thin crystals and we will show how a thin crystal can be advantageous for use as a polarimeter placed at the focus of a grazing incidence telescope. An instrument of this type will be flown on the Spectrum X-Gamma mission. We will conclude by comparing the expected sensitivity of the Spectrum-X-Gamma polarimeter with that of OSO-8.

2. THEORY OF CRYSTAL POLARIMETER OPERATION

A crystal oriented at 45° to an incident linearly polarized x-ray beam acts as a perfect polarization analyzer for photons with energies that satisfy the condition for Bragg reflection,

$$E = \frac{nhc}{2d \sin 45°} \tag{1}$$

In Eq.(1) E is the energy of the photon, n the diffraction order, h Planck's constant, c the speed of light, and d is the crystal lattice spacing. The crystal preferentially reflects photons with electric vectors perpendicular to the plane of incidence. These diffracted x-rays may then be detected by a proportional counter. If the crystal and detector combination is rotated around the line of sight to a linearly polarized x-ray beam, the detected signal will

*This work was performed under the auspices of the U.S. Department of Energy by Lawrence Livermore National Laboratory under Contract No. W-7405-ENG-48.

be sinusoidally modulated at twice the crystal rotation frequency. The degree of polarization is directly proportional to the amplitude of modulation, and the position angle of the electric vector is determined from the phase of the modulated signal.

3. BRAGG REFLECTION IN MOSAIC CRYSTALS

The peak reflection efficiency of nearly perfect crystals may be 50% or higher but only within a narrow energy bandwidth extending over a small fraction of an electron volt. Although such energy resolution is essential to x-ray spectroscopy, it is a hindrance to x-ray polarimetry because the majority of stellar sources emit weak continuum flux. To maximize the photon flux collected, the energy bandwidth can be broadened by utilizing imperfect crystals. An ideally imperfect crystal consists of a randomly oriented mosaic of small crystal domains. Each crystal domain has a regular atomic structure and may be thought of as a perfect crystalet. The crystalets are thin compared to the photoelectric absorption length in the crystal , allowing an x-ray to traverse many domains until it encounters one properly oriented for Bragg reflection. The random orientation of the small crystal domains greatly improves the possibility for simultaneous reflection of a range of photon wavelengths.

The rate at which x-rays are Bragg reflected from a flat crystal that is illuminated by continuum radiation at an angle θ_B is given by[3]

$$S(E_B) = I(E_B)\epsilon(E_B)A(E_B)\cot\theta_B\Delta\Theta(E_B)\ \ (ph/s) \tag{2}$$

where E_B is the energy that satisfies the Bragg condition at θ_B, $I(E_B)(keV\,cm^{-2}s^{-1}keV^{-1})$ is the x-ray continuum intensity, ϵ is the detector efficiency, A the projected area of the crystal, and $\Delta\Theta(E_B)$ is the integrated reflectivity. For fixed E_B,

$$\Delta\Theta(E_B) = \int_{\theta_1}^{\theta_2} R(\theta, E_B)d\theta \tag{3}$$

where $R(\theta, E_B)$ defines the reflectivity of the crystal as a function of angle for energy E_B and is commonly called the crystal rocking curve over the Bragg angle range from θ_1 to θ_2. The maximum value of R is the peak reflectivity of the crystal. It is clear from Eq. (2) that the number of reflected photons is directly proportional to $\Delta\Theta$ which should be maximized to detect weak stellar x-ray fluxes. A crystal will show high integrated reflectivity provided that the crystal domains are sufficiently misaligned and the size of the domains is small (see section 5.). A direct measure of the misorientation of the crystal domains is termed the mosaic spread, which is simply the angular width at half maximum of $R(\theta, E_B)$.

The integrated reflectivity of an ideal mosaic crystal illuminated with unpolarized radiation is given by[4,5]

$$\Delta\Theta(E_B) = \frac{N^2F^2{r_o}^2}{4\mu\sin 2\theta_B}\left[\frac{hc}{E_B}\right]^3(1+\cos^2 2\theta_B). \tag{4}$$

In Eq. (4) μ is the absorption coefficient at energy E_B, r_o is the classical electron radius, N the number of scattering cells per unit volume, and F is the crystal structure factor, or the number of scattering electrons per cell. Bragg reflection or coherent scattering is thus most efficient for crystals with well-defined crystal planes of high electron density. Photoelectric absorption is a competing effect but can be minimized by choosing scattering atoms with photoelectric cross sections that are small compared to their cross sections for coherent scattering. The latter is proportional to $F^2{r_o}^2$.

When polarized radiation is incident on a mosaic crystal, the angular dependence of the integrated reflectivity is given by

$$\Delta\Theta(E_B) = \frac{N^2F^2{r_o}^2}{2\mu}\left[\frac{hc}{E_B}\right]^3\left[\frac{1}{\sin 2\theta_B} - \frac{\sin 2\theta_B}{2}(1+P\cos 2\phi)\right]. \tag{5}$$

Here, P is the fractional polarization of the incident beam, and ϕ is the azimuthal angle measured between the plane of incidence and the plane formed by the polarization vector and the direction of the incident photon.

For the case of $\theta_B = 45°$,

$$\Delta\Theta(E_B) = \frac{N^2F^2{r_o}^2}{4\mu}\left[\frac{hc}{E_B}\right]^3(1-P\cos 2\phi). \tag{7}$$

Table 1[6] lists the theoretical values of the integrated reflectivity at 45° for several crystalline substances. It shows that tungsten disulfide, graphite, and lithium hydride have very high reflectivities. In practice, we have come close to obtaining the predicted theoretical value for graphite[7]. Natural crystals of molybdenum disulfide (MoS_2) also have a measured integrated reflectivity which approaches the maximum theoretical value shown in the Table 1. The latter is half that of graphite and is applicable at a lower energy where it becomes more difficult to operate with conventional sealed proportional counters. Extensive efforts to develop large mosaic tungsten disulfide crystals have been unsuccessful. Large crystals of lithium hydride are readily available, but they do not exhibit the high integrated reflectivity listed in Table 1. The best integrated reflectivity obtained to date for lithium hydride is about a factor of two less than that for graphite.

TABLE 1

Maximum Integrated Reflectivities

Crystal	$Energy_{45^\circ}$ (kev)	$\Delta\Theta \times 10^4$ (radians)
WS_2	1.40	15.0
MoS_2	1.43	8.3
PET	2.01	4.3
Graphite	2.61	15.9
Calcite	2.89	3.5
LiH	4.3	35.0
LiF	4.35	5.2

4. THE MOSAIC GRAPHITE CRYSTAL POLARIMETER ON OSO-8

Both theoretical and experimental studies show that a graphite mosaic crystal is the best choice for a crystal polarization analyzer at energies above 1 keV where members of several important classes of x-ray sources (x-ray binaries, pulsars, bursters, etc.) are near their peak intensities. The 2d crystal lattice spacing of 6.7 $\AA$ in graphite corresponds to reflection by the (002) crystal planes and makes a flat graphite crystal panel sensitive at 2.6 keV in first order reflection and at 5.2 keV in second order. The energy bandwidth in first and second orders is primarily due to the mosaic spread intrinsic to the specific graphite crystal chosen. The graphite on the OSO-8 instrument had a mosaic spread of 0.8° which set the intrinsic bandpass at 0.04 keV and 0.08 keV in first and second order, respectively.

To reduce the background signal, the crystal panel on OSO-8 was curved to focus the diffracted x-rays into a detector with a small surface area. The use of a flat crystal inclined at 45° to the incident x-ray beam would have required an x-ray detector whose window area was comparable to the projected crystal area if all the intercepted flux was to be collected. The susceptibility to excessive cosmic ray induced background is high for large area detectors and may produce a poor signal-to-noise ratio even when viewing the strongest sources. This is shown in Fig.1. A matrix of graphite crystals $200\mu m$ - $300\mu m$ thick was mounted on the surface of a 30° sector of a paraboloid of revolution. This technique reduced the instrumental background counting rate by approximately a factor of 20.

The curvature of the crystal panel on OSO-8 encompassed a range of Bragg angles between 40° and 50° and increased the overall energy bandwidth of the crystal panel to 0.4 keV and 0.8 keV for first and second order Bragg reflections. This caused little concern since all presently known x-ray sources are continuum emitters and all models that suggest polarization indicate that at most, the polarization would be a slowly varying function of energy. In addition, the expanded bandwidth was still narrower than the energy resolution of the detector at these wavelengths and did not significantly increase the background counting rate. The crystal curvature does reduce the instrument's sensitivity to polarization. The small range of Bragg angles about 45° allows a small unmodulated signal to be transmitted continually. The degree of polarization measured by the OSO-8 polarimeters when illuminated by a monoenergetic 100% polarized x-ray beam was 96%. A modulation curve is shown in Fig. 2 and is in agreement with calculations.

OSO-8 was a spinning vehicle. Two graphite polarimeters as described above were aligned with the spin axis and viewed the sky along this axis. Fig. 3 shows the pulse height spectrum recorded during the 1976 observation of the Crab Nebula[8]. The first and second order peaks at 2.6 keV and 5.2 keV, respectively, are clearly shown. The dashed line represents the background counting rate measured while the instrument's field of view was earth-occulted. The favorable signal-to-background ratio is the result of the focusing by the curved crystal panels.

By means of pulsar phase analysis, the x-ray contribution from the nebula was separated from that of the Crab Pulsar[9]. Fig. 4 shows the average nebula counting rate obtained at 2.6 keV as a function of polarimeter rotation angle. The modulation due to the nebula polarization is clearly evident in the upper curve. The lower curve is the average 2.6 keV background counting rate which shows no statistically significant modulation. The modulation data in the upper curve leads to a polarization at 2.6 keV of $19.22\% \pm 0.92\%$ at a position angle of $155.77^\circ \pm 1.37^\circ$. Fig. 5 depicts the 2.6 keV and 5.2 keV polarization results. This is the first high precision x-ray polarization measurement obtained for any cosmic source and in excellent agreement with optical polarization measurements of the Crab Nebula[10].

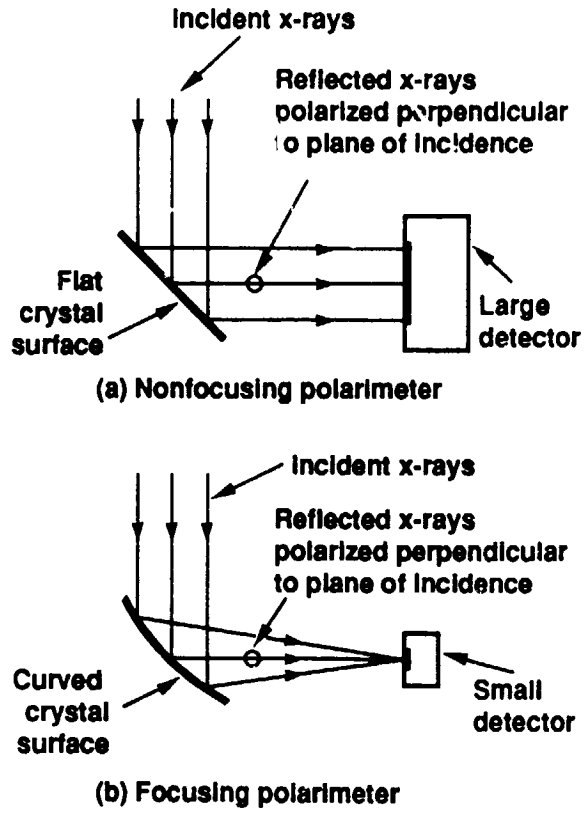

Figure 1. Conceptual diagram of nonfocusing and focusing polarimeters.

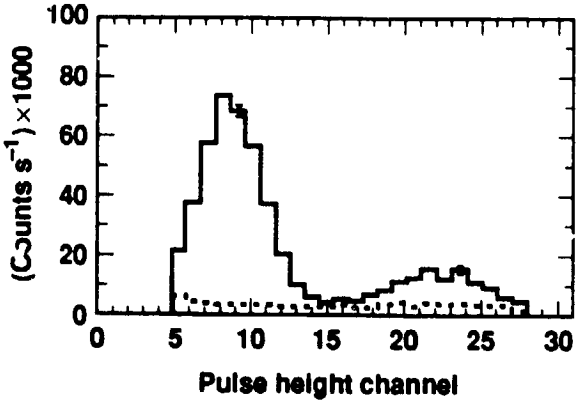

Figure 3. Pulse-height spectrum of the Crab Nebula. The first and second order peaks are clearly shown. The dashed line represents the background counting rate while the instrument's field- of-view was earth-occulted.

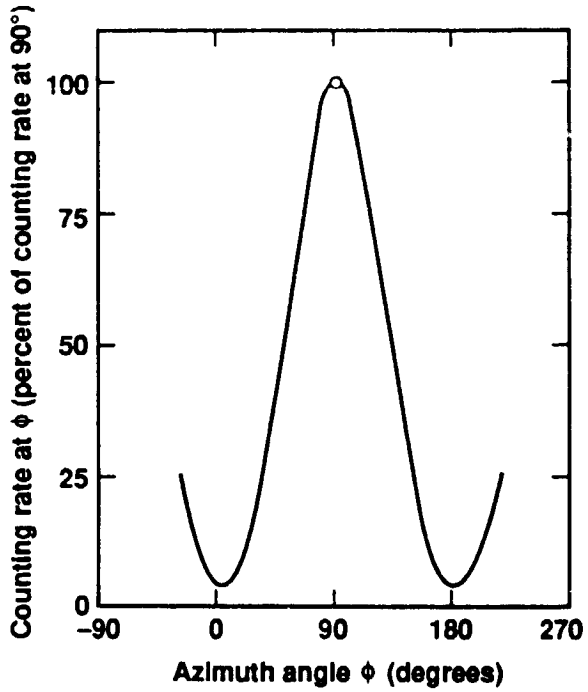

Figure 2. Modulation response of the pre-engineering model OSO-8 polarimeter, measured with a collimated beam of 5.2 keV (second order) x-rays.

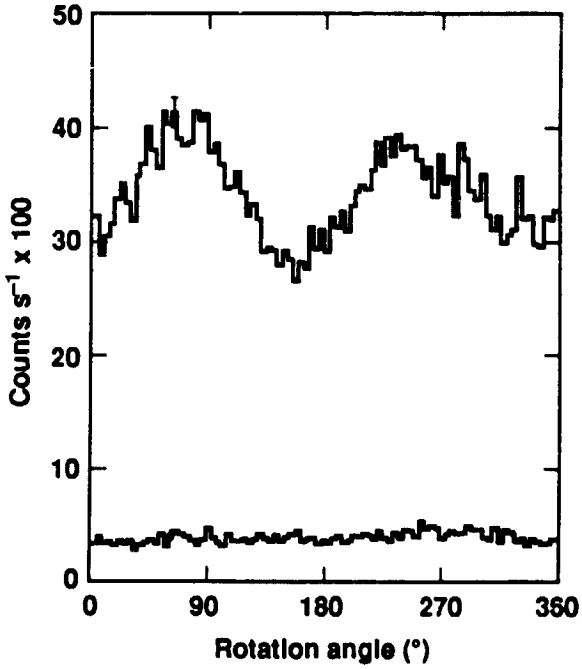

Figure 4. Modulation curves at 2.6 keV obtained during observations of the Crab Nebula(upper curve) and during the time when the instrument's field-of-view was earth-occulted (lower curve).

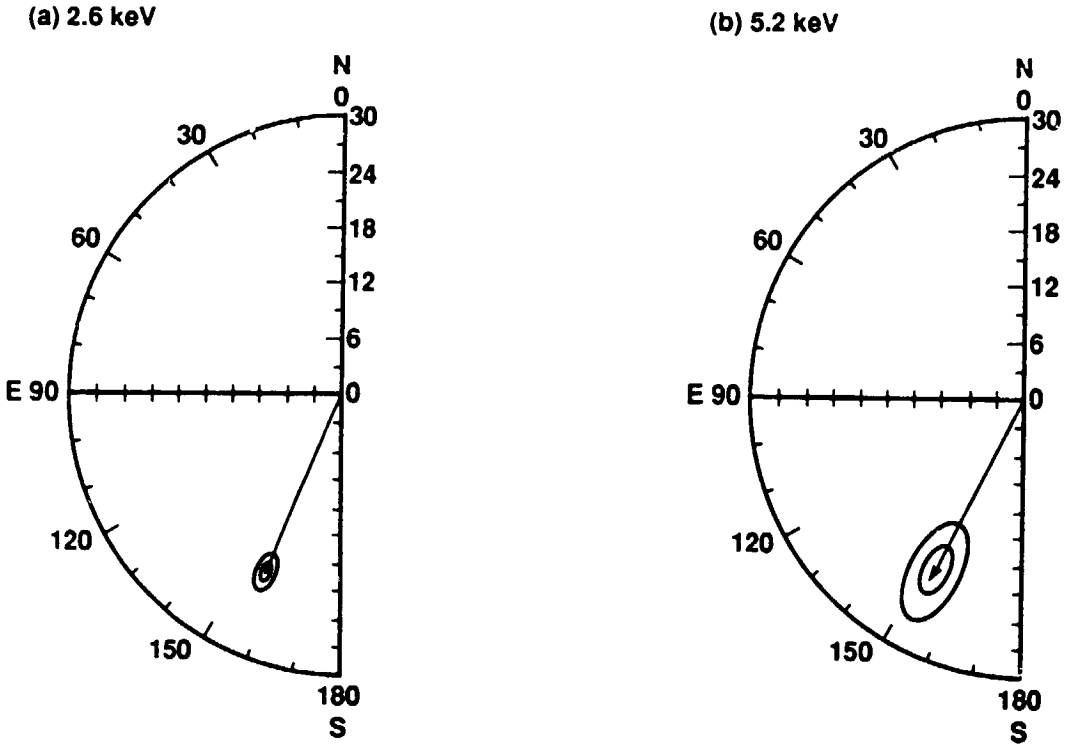

Figure 5. The polarization vectors of the Crab Nebula at (a) 2.6 keV and (b) 5.2 keV. Surrounding the vectors in order of increasing size are the 67% and 99% confidence contours. The radial scale is in percent.

5. X-RAY DIFFRACTION IN THIN CRYSTALS

X-ray diffraction occurs in a very thin surface layer of a crystal. Since it is a coherent process, x-rays that scatter from the atoms in the crystal add in phase, if the Bragg condition has been satisfied. As an incident x-ray beam proceeds through a crystal, its intensity is reduced by photoelectric absorption and by diffraction into a reflected beam. Even without absorption, the deeper parts of the crystal will diffract less than the upper parts because energy which is incident at the correct angle for diffraction is removed before it penetrates deep into the crystal. The strength of the incident beam diminishes appreciably with penetration. This reduction of the incident intensity is the phenomenon of extinction.

In a perfect crystal where the structure is uniform and regular throughout, extinction occurs because repeatedly reflected components of the incoming wave interfere destructively with the incoming travelling wave. At the Bragg angle this is so marked that reflection effectively takes place in a very thin surface layer with a depth of approximately 10^{-4} cm in graphite. Extinction due to a perfectly ordered structure of scattering cells is called *primary* .

Extinction will be much less apparent in the mosaic crystal. Intervening crystalets have different orientations and will not reflect at the same inclination of the incident beam. Since reflections from crystalets at different depths are not coherent, the forward travelling wave can penetrate further into the crystal. Extinction in this form is said to be *secondary* . If secondary extinction alone is to take place, mosaic crystalets must be small compared to the penetration distance for primary extinction. The crystal is then said to be *ideally imperfect* . Normally photoelectric absorption will prevent x-rays from penetrating a mosaic crystal to a depth where secondary extinction becomes too significant. When extinction is negligible, the integrated reflectivity reaches an upper limit which is defined by Eq.(4). It is convenient for the remaining discussion to rewrite this limit as $Q/2\mu$ where Q is

$$Q = \frac{N^2 F^2 {r_o}^2}{sin2\theta_B}\left[\frac{hc}{E_B}\right]^3 \frac{(1+\cos^2 2\theta_B)}{2} . \tag{7}$$

Zachariasen[11] has derived the integrated reflectivity as a function of the thickness of a mosaic crystal for varying values of Q accounting for the effects of secondary extinction. His formulation has been furthe. developed by Bacon and Lowde[12] who compare crystal properties for both x-ray and neutron diffraction. Using their general theory we have calculated the integrated reflectivity in the regime where mosaic crystals will be useful for x-ray polarimetry. These are depicted in Fig. 6 where the integrated reflectivity, $\Delta\Theta$, is plotted versus the crystal thickness, T_o for different limiting values of $Q/2\mu$. The abcissa in Fig. 6 is the product of the crystal thickness, T_o, Q, and $1/\gamma_o$ where γ_o is equal to $\sin\theta$ for Bragg reflection. The parameters in Fig. 6 have been normalized by η, which is the standard deviation of the crystal rocking curve. (The mosaic spread is $2.35 \times \eta$.) The solid lines in Fig. 6 represent the case of Bragg reflection. The dashed lines correspond to the case where diffracted x-rays are observed in transmission as shown in Fig. 7. This is called "Laue" diffraction and will occur if the thickness of a crystal is small with respect to the photoelectric absorption length. For the Laue case $1/\gamma_o$ equals $\cos\theta$.

Notice that $\Delta\Theta$ rises quickly and reaches its limiting value $Q/2\mu$ for Bragg reflection in strongly absorbing crystals, i.e., where secondary extinction is unimportant. For larger values of $Q/2\mu$ extinction causes the $\Delta\Theta$ to fall below $Q/2\mu$. For reference and use in further discussion, the value of $Q/2\mu$ for graphite with a mosaic spread of 0.8° at 2.6 keV $\approx 1.6 \times 10^{-3}$ radians. The calculations show that, due to secondary extinction, the limiting value of $\Delta\Theta$ is $\approx$ 18% lower than $Q/2\mu$. The Laue values for the integrated reflectivity also increase sharply, but ultimately decay with larger T_o as the effects of photoelectric absorption begin to dominate. The maximum of each Laue curve provides the optimum thickness for a mosaic crystal of given Q, μ, and η. Compton and Allison[13] as well as Zachariasen have derived the expression $T_o(optimum) = \gamma_o/\mu$ for the peak values ignoring the effects of secondary extinction. The results from the general theory plotted in Fig. 6 show that the optimum thickness falls below $T_o = \gamma_o/\mu$ when secondary extinction is included. The curves also indicate that at the thickness where $\Delta\Theta$ first reaches its limiting value in Bragg reflection, the $\Delta\Theta$ in transmission is approximately half that value.

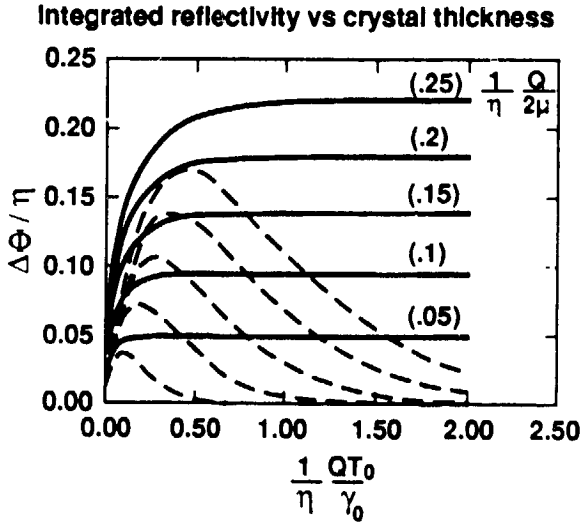

Figure 6. The integrated reflectivity, $\Delta\Theta$ from mosaic crystals as a function of thickness, absorption coefficient, structure factor, and mosaic spread. The solid lines are for Bragg reflection where $\gamma_o = \sin\theta$. The dashed lines are for the Laue transmission where $\gamma_o = \cos\theta$.

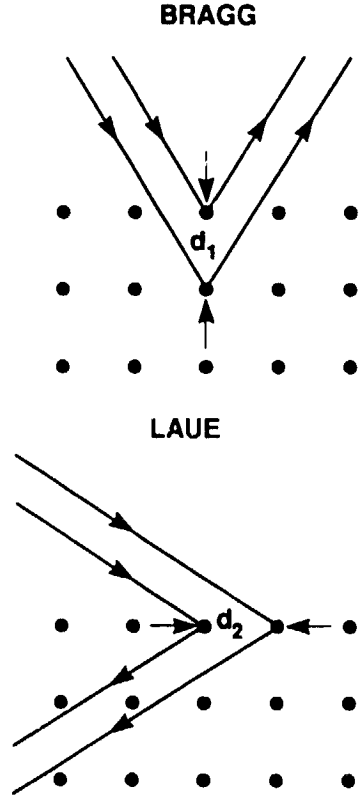

Figure 7. The ray geometry for Bragg reflection and Laue transmission.

6. THE GRAPHITE CRYSTAL POLARIMETER FOR SPECTRUM-X-GAMMA

We are currently applying the theory of thin crystal diffraction to the design of a new type of polarimeter which will be flown aboard the Soviet Spectrum X-Gamma spacecraft. This is called the focal plane stellar x-ray polarimeter (SXRP). In addition to a graphite crystal polarimeter, the SXRP incorporates a target of metallic lithium to exploit the polarization dependence of Thomson scattering. The lithium element operates over a broad band of energies extending from 4 to 12 keV or higher. In the SXRP design[14] shown in Fig. 8, a thin mosaic graphite crystal is mounted permanently above a lithium target. If the Laue geometry proves feasible experimentally, and the mosaic graphite crystal is cubic so that $d_1 = d_2$ in Fig. 7, then we will use the proportional counter behind the crystal(also used with the lithium polarimeter) to detect the diffracted Laue x-rays at 2.6 keV and 5.2 keV. In Fig. 8 we only show x-rays Bragg reflected into a proportional counter.

This combination will always be located in the focused x-ray beam permitting the observer to simultaneously obtain polarization data over the complete SXRP energy band from 2.6 keV to 12 keV. In addition this configuration will require less observing time to study the x-ray sources of interest and the well-defined x-ray image that is formed by the graphite crystal on the face of the imaging detectors can be used also to obtain direct x-ray aspect information during all of the polarimeter observations.

Using the information from Fig. 6 we have calculated the graphite crystal thickness that will provide the necessary integrated reflectivity for the polarization measurements at 2.6 keV while still allowing at least 75% of the x-rays with energies greater than 5 keV to be transmitted to the lithium scattering block. We have chosen to examine the diffraction properties of $20\mu m$ and $50\mu m$ thick crystals. In Table 2 we tabulate the parameters that are used in these calculations. The $20\mu m$ crystal corresponds to the thickness for the Laue geometry case that gives the optimum diffraction in transmission. The 50 μm crystal corresponds to the minimum thickness that yields the highest limiting value of $\Delta\Theta$ for the Bragg reflection case. These values are easily obtained from Fig. 6 and and the data in Table 2.

Notice that the sum of the Bragg and Laue integrated reflectivities at 2.6 keV is slightly greater for the $20\mu m$ crystal than for the $50\mu m$ crystal. The Bragg reflectivity is somewhat smaller in the $20\mu m$ crystal while the Laue contribution is higher in the $20\mu m$ crystal. This must be verified experimentally (see section 7) but the $20\mu m$ crystal is potentially the better choice for SXRP. It theoretically will maximize the total reflectivity while minimizing the absorption of x-rays at the energies required by the lithium scattering target. We have already produced a $25\mu m$ thick crystal and are currently characterizing these reflection properties. If crystals this thin do not prove to be robust enough, we will use $50\mu m$ thick samples. The transmission of a $50\mu m$ thick crystal oriented at 45° to the incoming beam is 75% at 5.2 keV and 93% at 7.8 keV, which is the energy for Bragg reflection in third order. At energies away from the Bragg peaks the transmission increases from 55% at 4 keV to 85% at 6 keV and 96% at 10 keV. Since the lithium polarimeter is ineffective below about 5 keV the graphite crystal will have only a small effect on the performance of the lithium polarimeter.

As in our OSO-8 design the 2.6 and 5.2 keV x-rays are sufficiently separated in energy to be easily resolvable by the proportional counters. The modulation factor for SXRP is ≈ 0.99 because the x-rays from the the grazing incidence telescope form a converging beam that deviates by only a few degrees from the 45° required by a perfect polarization analyzer. The nominal design parameters for the Bragg crystal polarimeter on SXRP, which do not include the Laue contribution are listed in Table 3.

7. DEVELOPMENT OF THIN GRAPHITE CRYSTAL POLARIMETER

7.1. Thinning pyrolytic graphite

In order to produce the necessary thin wafers of pyrolytic graphite, we have developed a two step process for thinning. One can cleave the bulk material by hand using a single edged razor blade and microscope, being careful to align the blade parallel with the cleavage planes of the material. However, this procedure usually leads to a heavily fractured bent wafer.

Further thinning is accomplished with a successive reduction technique. Starting with a wafer of known thickness (0.01 inches thick in this case), one adheres the wafer to a carbon block using melted wax[15]. It is essential that the adhesion is limited to the bottom surface only, and that no wax extrudes along the sides of the graphite wafer. After cooling the block, one can then lift thin layers of graphite crystal off the surface of the wafer using adhesive tape. We observed that each *lift* corresponds to a reduction in thickness of approximately 0.001 inches ($25\mu m$). With this technique, a wafer of unfractured pyrolytic graphite remains stuck to the carbon block and can be dismounted at any time by heating the carbon block and sliding the wafer off. The adhesive wax is then removed from the thin wafer by soaking it in a chlorinated hydrocarbon solvent such as trichlorethane. With this technique we have already produced wafers as thin as $25\mu m$ that have lateral dimensions of 1 cm by 2.5 cm.

TABLE 2

Thin Mosaic Graphite Crystals For Polarization Measurements

Crystal Properties

2d spacing : 6.7 Å	N : 2.859×10^{22} cm^{-3}
F : 16.6	η : 5.94×10^{-3} radians
Q (2.6 kev) : 0.97 cm^{-1}	Q (5.2 keV) : 0.12 cm^{-1}
μ (2.6 keV) : 304 cm^{-1}	μ (5.2 kev) : 42 cm^{-1}

Crystal Thickness (μm)	Energy (keV)	Bragg (radians)	$\Delta\Theta$ Laue (radians)	Sum (radians)	X-ray Transmission (%)
20	2.6	1.2×10^{-3}	1.0×10^{-3}	2.2×10^{-3}	42
	5.2	6.2×10^{-4}	3.0×10^{-4}	9.2×10^{-4}	89
50	2.6	1.3×10^{-3}	6.5×10^{-4}	2.0×10^{-3}	12
	5.2	9.5×10^{-4}	6.9×10^{-4}	1.6×10^{-3}	74

TABLE 3

Design Parameters for SXRP Graphite Crystal Polarimeter

Energy keV	$\Delta\Theta$ Radians	Telescope Area cm^2	Detector Efficiency	Detector Resolution keV	Crab Intensity keV/(kev-cm^2-s)
2.6	1×10^{-3}	1100	0.9	0.68	3.8
5.2	5×10^{-4}	1374	0.9	0.96	1.9

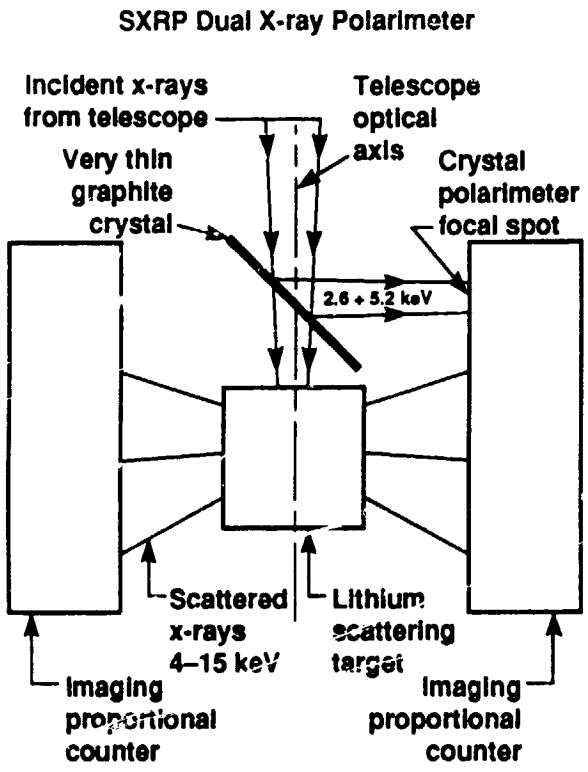

Figure 8. The schematic of the dual polarimeter design for SXRP.

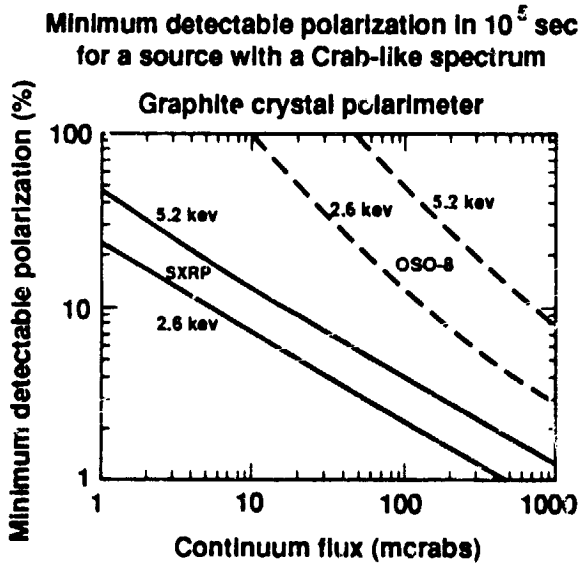

Figure 10. The sensitivities of the SXRP and OSO-8 graphite crystal polarimeters for sources with Crab-like spectra. The observation time is 10^5 seconds.

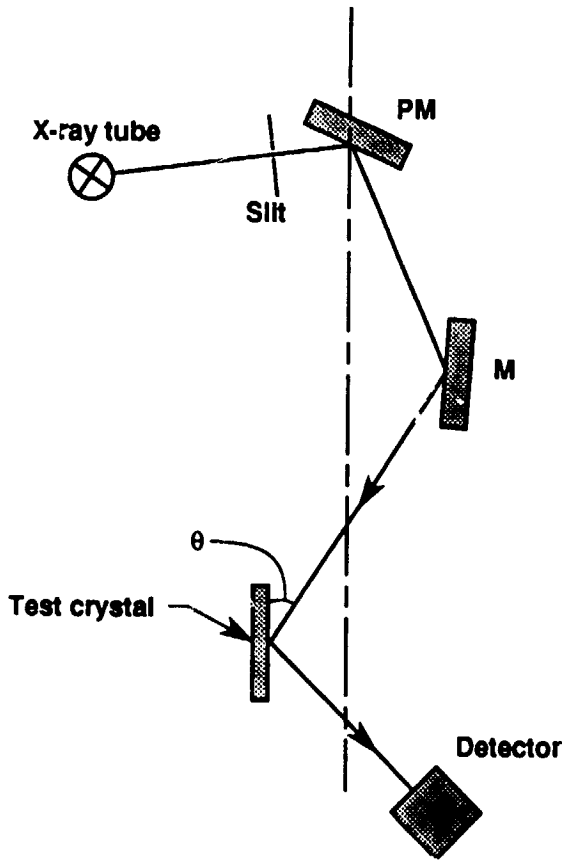

Figure 9. The triple crystal set-up in the dispersive geometry. PM and M define an incident x-ray beam to probe the test crystal.

7.2. Measuring the integrated reflectivity, mosaic spread and x-ray transmission

The crystal parameters for a mosaic crystal are best measured using a triple axis spectrometer as described by Christensen et al.[16] This technique eliminates the need for a long x-ray beam line to produce a collimated monoenergetic x-ray source. As shown in Fig. 9 two perfect crystals, labelled PM and M, are configured in a dispersive double-crystal geometry[13] to produce a well collimated ($<<$ 1 arc minute), monoenergetic ($\Delta E \leq 5eV$) x-ray beam. This beam is then used as a probe to measure the mosaic spread and integrated reflectivity of the sample crystal. Since the mosaic spread of the pyrolytic graphite will be $\approx 0.5° - 0.8°$ the collimation and narrow energy band provided by ADP or silicon crystals are sufficient for characterizing the mosaic properties. We are currently assemblying the spectrometer and will begin testing shortly.

8. EXPERIMENT SENSITIVITY

8.1. Statistics

It is important to be able to estimate for several representative x-ray sources the minimum level of polarization that could be detected as a function of integration time. Since the amplitude of modulation at twice the rotation frequency of the polarimeter and hence, the polarization, is a positive definite quantity[17], statistical fluctuations in the data from even an unpolarized source can appear as a positive detection. If a source is on axis and unpolarized and if the detected data are considered to be drawn from a broad band noise source characterized by a mean number of counts per azimuthal phase bin, $\overline{S}$, and a variance of σ^2, then the probability of measuring a given fractional polarization amplitude of modulation a or greater by chance is given by

$$\Pi(a' \geq a) = \exp \frac{-n\overline{S}^2 a^2}{4\sigma^2} \tag{8}$$

where n is the number of azimuthal phase bins. In the limit where the data are Poisson distributed, ($\sigma^2 = \overline{S}$), this reduces to

$$\Pi(a' \geq a) = \exp \frac{-Na^2}{4} \tag{9}$$

where $N = n\overline{S}$ is the total number of counts measured. For the purposes of this discussion, we accept that a detection is significant if there is a 1% probability of measuring a given amplitude of modulation or greater by chance. Eq (9) then implies a minimum detectable modulation of $a = 4.29/\sqrt{N} \simeq 3\sqrt{2/N}$. It is then straightforward to express the minimum detectable polarization P in terms of the source counting rate, S, the background counting rate B and the total observing time T as

$$P = 4.29\left[\frac{S+B}{T}\right]^{\frac{1}{2}} \frac{1}{mS} \tag{10}$$

where m is the modulation factor.

8.2 Sensitivity of the OSO-8 and SXRP polarimeters

Using the data in Table 3, we have estimated the sensitivity of the SXRP for a number of sources and compared it to that of OSO-8. Fig. 10 shows the sensitivity of the SXRP and OSO-8 graphite crystal polarimeters for a Crab Nebula-like source. Table 4 lists the sensitivities for a number of important sources. For the strong sources where background is a negligible contribution to the total signal for both polarimeters, the SXRP polarimeter is approximately three times more sensitive than the OSO- 8 polarimeter because the effective area of the grazing incidence telescope on Spectrum-X-Gamma has about 10 times the area at 2.6 keV and 5.2 keV than the projected area of the OSO-8 crystals. For the weaker sources, the improvement in sensitivity becomes more dramatic primarily because the x-ray image reflected by the crystal in SXRP is confined to a small number of pixel resolution elements in the imaging proportional counters. The background contribution remains negligible for SXRP where it did not for the OSO-8 instrument.

TABLE 4

Minimum Detectable Polarization in 10^5 Seconds For SXRP and OSO-8

Source	Observing Time (10^5sec)	SXRP		OSO-8	
Energy(keV)		2.6	5.2	2.6	5.2
Binary X-Ray Pulsars					
Her X-1	1	3.3	4.1	29.0	
0900-40	1	2.8	3.7		
GX1+4	1	4.3	5.4		
4U1626-67	2	3.4	4.9		
4U1223-62	2	3.8	3.1		
Cen X-3	1	1.8	2.4	9.6	15.5
SMC X-1	1	3.0	4.6		
Black Holes Candidates					
Cyg X-1 (Low State)	1	2.5	8.1		
Cyg X-1 (HI-State)	1	0.8			
Supernova Remnants					
Crab Nebula	2	0.5	1.1		
Radio Pulsars					
Crab Primary Pulse	2	6.0	12.7	17.0	42.0
Leading edge	2	8.0	17.0	22.0	54.0
Trailing edge	2	9.4	19.0	26.0	62.0
QPO's					
Sco X-1	1	0.7	1.9		
Cyg X-2	1	1.5			
Non-Pulsating Binaries					
CYG X-3	1	2.1			
Seyferts, BL Lacs, and QSOs					
NGC4151	6	9.6	6.0		
MK501	6	5.7	11.6		
MK421	6	4.6	10.7		
Cen A	4	3.8	2.7		
3C273	6	3.8	5.5		

9. SUMMARY

We have reviewed the theory of x-ray diffraction as it pertains to the design of a Bragg crystal polarimeter. The performance of the OSO-8 polarimeter was used to exemplify the merits of the rotating mosaic crystal technique. A more sensitive graphite polarimeter called the SXRP is being built for the Spectrum-X-Gamma mission and its novel design is discussed. The sensitivity of the SXRP is compared to that of OSO-8.

9. ACKNOWLEDGEMENTS

The authors wish to thank D. Van Lue, G. Power, T. Stack, S. Compton, and R. Morales for greatly assisting in the design and fabrication of the spectrometer and calibration facility that will be used to characterize the SXRP polarimeter. We also wish to thank Y. Wai and L. Melkonian for a critical reading of the manuscript.

10. REFERENCES

1. R. Novick, H.L. Kestenbaum, K.S. Long, E.H. Silver, M.C. Weisskopf, and R.S. Wolff, Highlights of Astronomy, Edith A. Mueller, Editor, D. Reidel, Dordrecht, Netherlands, Vol. 4, 91, 1976.

2. R. Novick, M.C. Weisskopf, E.H. Silver, H.L. Kestenbaum, K.S. Long, and R.S. Wolff, in *Proceedings of the Eighth Texas Symposium on Relativistic Astrophysics* , New York Academy of Sciences, 312, 1977.

3. E. H. Silver, *X-Ray Polarization of the Crab Nebula and Pulsar and Centaurus X-3 and Hercules X-1 Pulsars*, Ph.D. Thesis, Columbia University, 1978.

4. C.G. Darwin, Phil. Mag., 27, 881, 1914.

5. R.W. James, The Optical Principles of the Diffraction of X-Rays, G. Bell and Sons, Ltd., London, 1948.

6. J.R. Angel and M.C. Weisskopf, Astron. J., 75, 231, 1970.

7. H.L. Kestenbaum, Appl. Spectrosc., 27, 454, 1973.

8. M.C. Weisskopf, E.H. Silver, H.L. Kestenbaum, K.S. Long, and R. Novick, Ap. J. 220, L117, 1978.

9. E.H. Silver, M.C. Weisskopf, H.L. Kestenbaum, K.S. Long, R. Novick, and R.S. Wolff, Ap. J. 225, 221, 1978.

10. J.H. Oort and T. Walraven, Bull. Astron. Inst. Neth., 12, 285, 1956.

11. W.H. Zachariasen, Theory of X-Ray Diffraction in Crystals, Wiley, New York, 1944.

12. G.E. Bacon and R.D. Lowde, Acta Cryst., 1, 303, 1948.

13. A.H. Compton and S.K. Allison, X-Rays in Theory and Experiment, Van Nostrand, New York, 1935.

14. R. Novick, E. Silver, M. Weisskopf, C. Martin, T. Hamilton, G. Chanan, R. Elsner, G. Manzo, E. Costa, G. Fraser, G.C. Perola, in *Proceedings of SPIE's 33rd Annual International Symposium on Optical and Optoelectronic Applied Science and Engineering*, 6-11 August, 1989.

15. Red Sticky Wax, L.D. Caulk Company, Milford, Delaware 19963.

16. F.E. Christensen, H.W. Schnopper, E.H. Silver, and N.J. Westergaard, in *Proceedings of the ESA Workshop on a Cosmic X-Ray Spectroscopy Mission*, 24-26 June 1985, Lyngby, Denmark.

17. E.H. Silver, R. Novick, and M.C. Weisskopf, SPIE, Vol.112, Optical Polarimetry, 45, 1977.

DISCLAIMER